HARP Collaboration

HARP Memo 08-101
4 February 2008
corrected 29 March 2008
updated 3 October 2008
http://cern.ch/harp-cdp/T9beammuons.pdf

Fraction of muons in the T9 pion beams

V. Ammosov, A. Bolshakova, I. Boyko, G. Chelkov, D. Dedovitch, F. Dydak, A. Elagin, M. Gostkin, A. Guskov, V. Koreshev, Z. Kroumchtein, Yu. Nefedov, K. Nikolaev, J. Wotschack, A. Zhemchugov

CERN-HARP-CDP-2008-001
04/02/2008

Abstract

In the T9 beam line, the beam instrumentation does not permit the separation of pions from muons. For a correct pion interaction cross-section, the flux of beam muons must be subtracted from the flux of pion-like particles incident on the target. In this memo, data from the beam instrumentation and the beam-muon identifier in 'empty-target' runs are analyzed in order to measure the fraction of beam muons incident on the target, in the pion beams from 3 to 15 GeV/c.

Contents

1 Introduction **2**

2 Characteristics of the beam-muon identifier **2**

3 Data sample and beam preselection **4**

4 Strategy of pion–muon separation **4**

5 Calibration of the photomultiplier response **4**

6 Hadrons versus muons in the beam-muon identifier **5**

7 Muon fraction in T9 pion beams **11**

1 Introduction

While protons in the T9 beam line are well separated from pions by the beam instrumentation (two threshold Cherenkovs and TOF scintillators), muons are not. For a correct pion interaction cross-section, the flux of beam muons must be subtracted from the flux of pion-like particles incident on the target.

In this memo, we describe our method to separate muons from pions. Because of the use of variables with large discrimination potential, a rather clean separation is possible with little reliance on Monte Carlo simulation.

In Section 7, we state our results and compare them with the results reported by 'official' HARP [1].

2 Characteristics of the beam-muon identifier

The schematic layout and a photograph of the beam-muon identifier are shown in Fig. 1. The characteristics of its instrumentation are summarized in Table 1.

Table 1: Instrumentation characteristics of the beam-muon identifier

Thickness of front iron absorber [mm]	400
Thickness of iron slabs [mm]	50
No. of sampling sections	5
Thickness of sampling sections [mm]	450, 200, 200, 150, 150
No. of scintillator planes	5
Scintillator counters per plane	6
Scintillator counter dimensions [mm]	$1400 \times 100 \times 6$
Type of scintillator	BC 408
No. of PMTs	$5 \times 6 \times 2 = 60$
Type of PMTs	2 inch EMI 9839A
Type of ADCs	CAEN QDC V 792

The beam-muon identifier is horizontally shifted with respect to the z-coordinate axis, with a view to accommodating the horizontal bending of the beam particles in the experiment's dipole spectrometer magnet.

The beam-muon identifier's vertical and horizontal widths are large enough for an adequate containment of hadron showers.

The total iron thickness of the beam-muon identifier is 1150 mm ($\sim 5.9\ \lambda_{\mathrm{int}}$). The longitudinal segmentation into five sections permits a good separation between muons and hadrons.

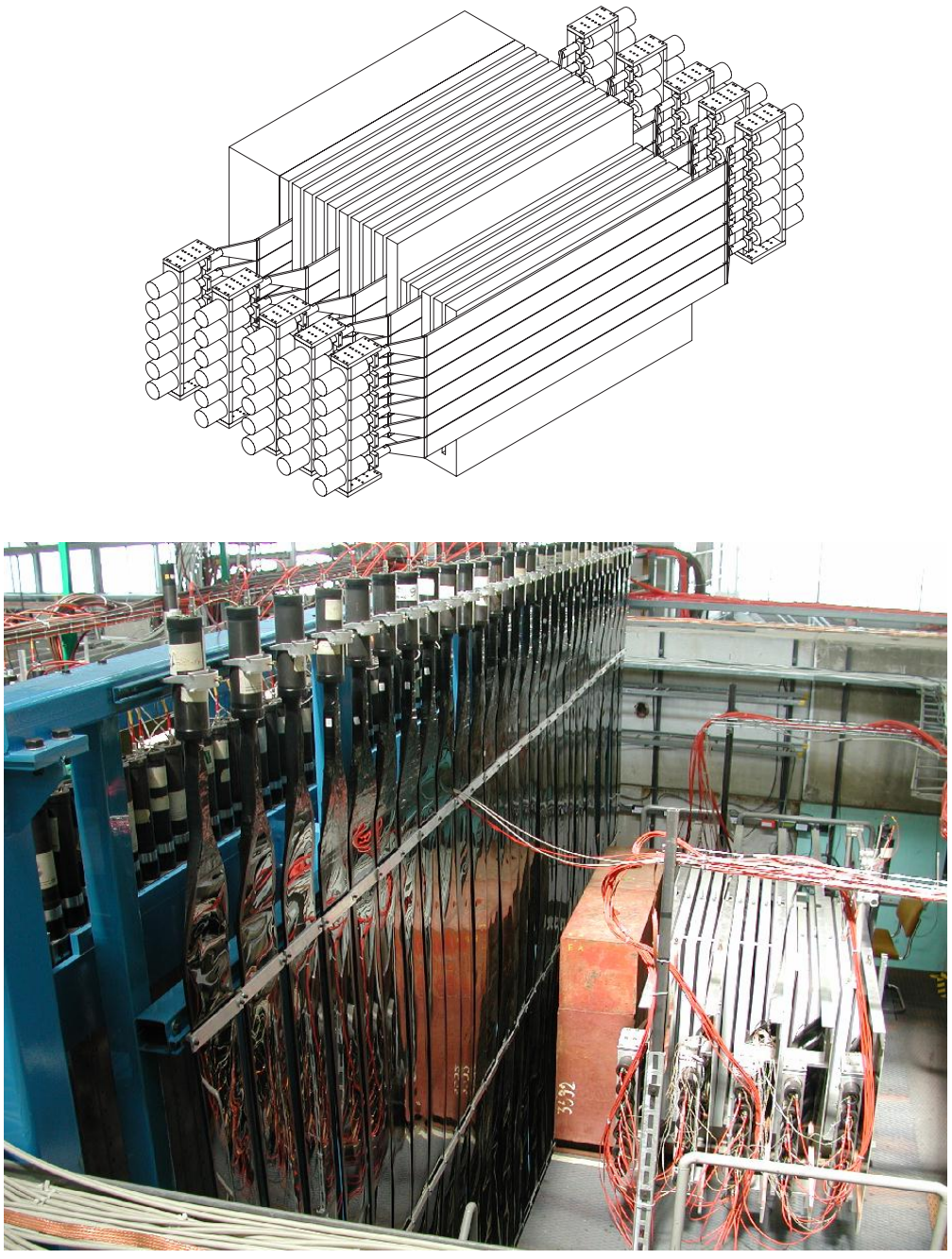

Figure 1: Schematic layout (upper panel) and photograph (lower panel) of the beam-muon identifier; particles are entering from the left.

3 Data sample and beam preselection

In this analysis, 'empty-target' runs are used. Only events with a 'downscale trigger bit' are considered (except for the calibration of the PMT response of the beam-muon identifier and the characterization of the hadron–muon discrimination[1], described in Sections 5 and 6), with a view to avoiding a bias in the beam particles.

Beam particles are selected as follows. They must be identified as either proton or else as pion or muon[2] by means of the beam Cherenkov counters. The particle velocity measured in the beam TOF counters must be consistent with the particle type from the Cherenkov identification. The trajectory of the beam particle must be unambiguously reconstructed by the beam MWPC's.

Beam particles passing these selections are classified as 'pions/muons' or 'protons'. For example, in the +8.9 GeV/c beam, the fraction of 'pions/muons' of all beam particles is $\sim 30\%$.

4 Strategy of pion–muon separation

The strategy of pion–muon separation rests on the following feature that distinguishes pions from muons: in the five scintillator planes of the beam-muon identifier in the longitudinal direction, the showering profile of pions strongly fluctuates, while the minimum-ionizing pulseheight of muons exhibits smooth uniformity. This feature permits the determination of the muon fraction with little reliance on Monte Carlo simulation.

5 Calibration of the photomultiplier response

First, the signal amplitudes of the 60 PMT signal amplitudes were equalized by requiring that muons give the same response.

The equalization procedure was performed iteratively. Initially, the PMT response to muons was set to some reasonable starting value. Then a rather clean sample of muons was selected requiring that the sum of signals in a scintillator plane was consistent with the minimum-ionizing pulseheight, for four planes out of five (excluding the plane to which the PMT under consideration belonged). From this sample of muons more precise PMT equalization constants were determined. Then the procedure was repeated until convergence.

The PMTs' response to muons, after convergence, is shown in Fig. 2. The histogram entries represent the most probable muon response. The r.m.s. spread of the response per PMT is about 20% (14% for the combined response of the two PMT's of the same counter).

Only 60% of the PMTs could be calibrated in the way described. For the remaining ones

[1]For these tasks, the requirement of the 'downscale trigger bit' was dropped with a view to benefitting from muons that were recorded with a physics trigger bit.

[2]Electrons also cannot be separated from pions and muons.

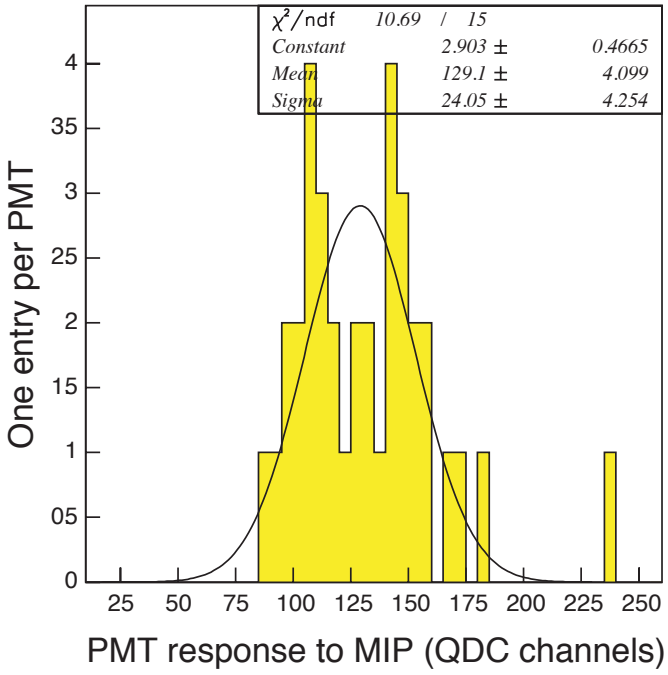

Figure 2: Most probable charge response of the PMTs of the beam-muon identifier to muons.

the statistics of muons were not sufficient. We use in these cases the average response (129.1 ADC channels) from PMTs with sufficient statistics.

For every event, the ADC amplitudes of each PMT channel are divided by the PMT's most probable response to muons. The resulting response to a minimum-ionizing particle in one layer is about 2, and the sum of all signals produced by a minimum-ionizing particle in the whole beam-muon identifier is about 10.

Figure 3 shows calibrated muon charge responses in the five layers (the layers are very similar in their behaviour). For this plot, the following 'tight muon selection' is employed: $R^2 > 225$ mm^2 where $R^2 = x^2_{\rm impact} + y^2_{\rm impact}$ is the particle's squared impact radius at the target, and $1.5 < Q < 2.7$ in each of the four other layers where Q is the observed calibrated charge in the layer. Noteworthy are the Landau tail and the good average efficiency per layer for the muon charge of 98.5% which bears witness to the good functioning of the beam-muon identifier.

6 Hadrons versus muons in the beam-muon identifier

In this section, data from the +8.9 GeV/c beam are shown.

Figure 4 shows the map of average charges in the 30 scintillators of the beam-muon identifier, deposited by muons (upper panel; a selection of muons with the cut $\xi < -1.0$ is applied, see below) and by protons (lower panel). Muons tend to produce a uniform response along

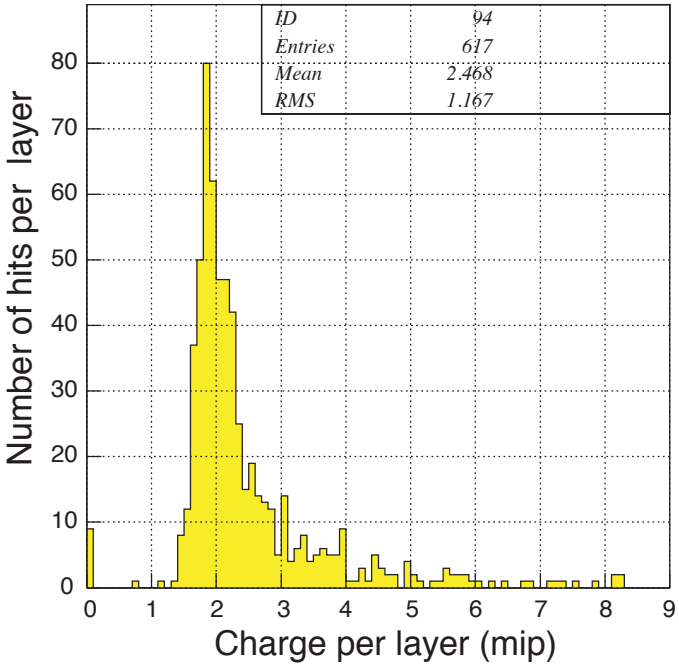

Figure 3: Calibrated muon charge responses in the five layers.

the calorimeter and the signals cluster around the nominal beam trajectory. By contrast, the signals from protons tend to exhibit a large longitudinal variation and a large transverse spread.

The obvious differences between muons and protons in the charge depositions are exploited by the following two variables:

1. the total energy deposition '$ETOT$', represented by the sum of the charges of all 60 PMT's) and

2. the longitudinal energy fluctuation 'RMS', represented by the the r.m.s. spread of the charges deposited in the five layers of the beam-muon identifier.

The transverse spread of the deposited charges is strongly correlated with the longitudinal charge fluctuation. It was found that adding this variable did not improve the discrimination.

The distributions of the discriminating variables $ETOT$ and RMS are shown in Figs. 5 and 6. The muon signature shows up clearly when the proton beam is compared with the pion/muon beam. The distribution of RMS is shown for the range $8 < ETOT < 14$ with a view to enhancing the muon fraction.

The hadron–muon separation is apparent in the 2-dimensional plots $ETOT$ versus RMS, see Figs. 7 and 8. In the latter plot, muons stick out by their concentration at medium $ETOT$ and small RMS.

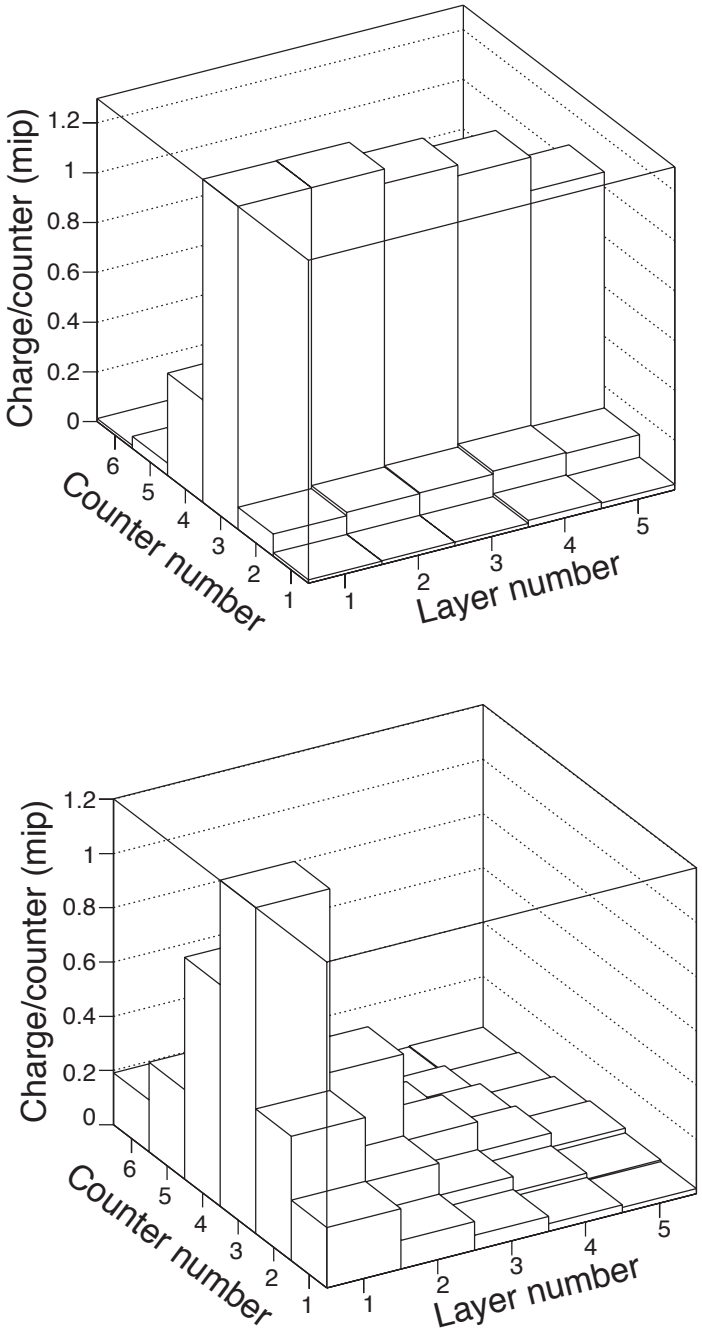

Figure 4: Average charges deposited in the scintillators of the beam-muon identifier by muons (upper panel), and by protons (lower panel).

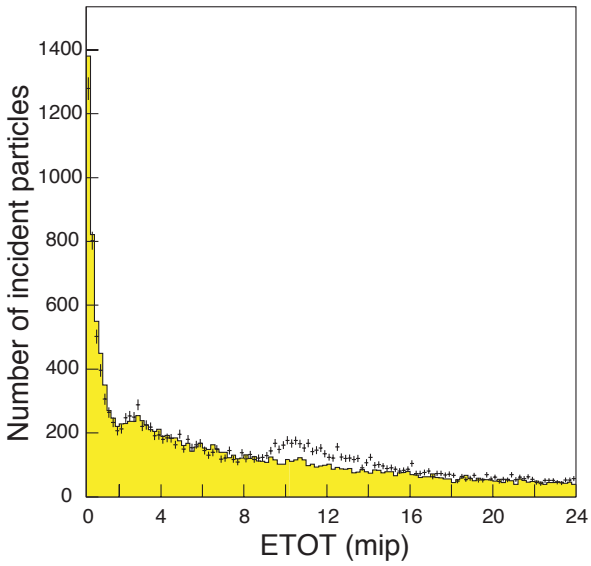

Figure 5: Total energy deposition $ETOT$ for protons (yellow/shaded histogram) and pions/muons (crosses); the first bin ($ETOT = 0$) is suppressed; the proton entries are scaled to match approximately the hadronic component of pions/muons.

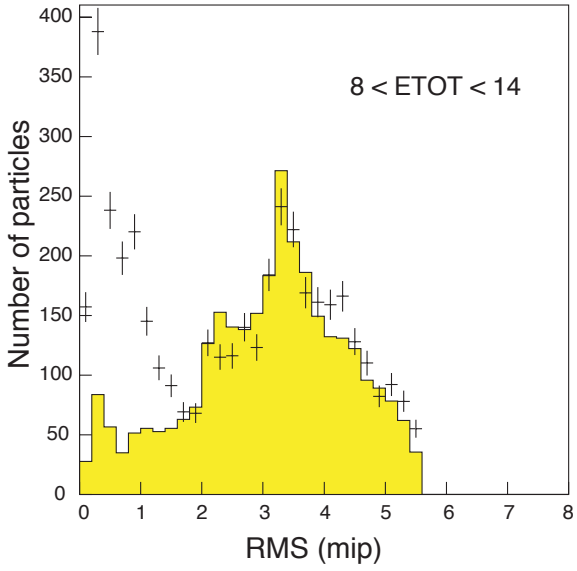

Figure 6: Fluctuation RMS of the energy deposition in the five layers of the beam-muon identifier for protons (yellow/shaded histogram) and pions/muons (crosses), for events with $8 < ETOT < 14$; the proton entries are scaled to match approximately the hadronic component of pions/muons.

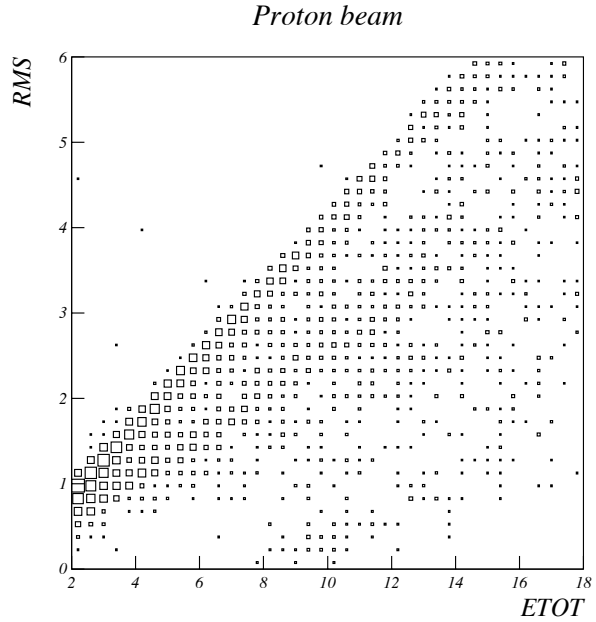

Figure 7: Longitudinal energy fluctuation RMS versus total energy deposition $ETOT$ for protons.

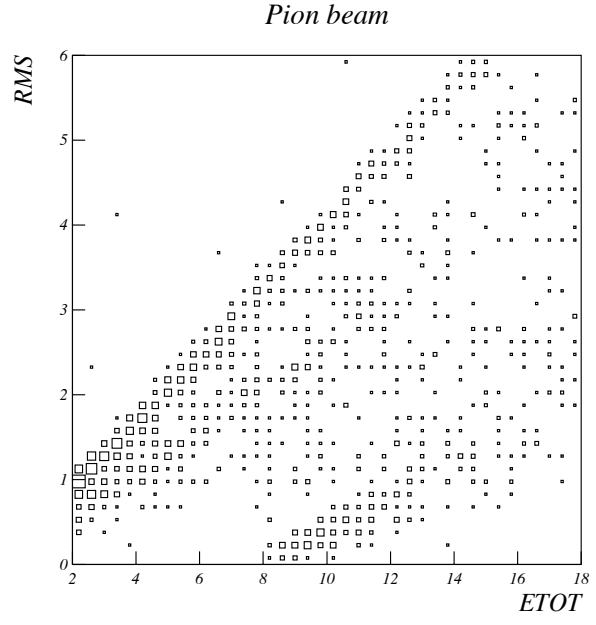

Figure 8: Longitudinal energy fluctuation RMS versus total energy deposition $ETOT$ for pions/muons.

The correlation between $ETOT$ and RMS of muons, clearly visible in Fig. 8, is well represented by the one-dimensional discriminating variable

$$\xi = RMS - 0.25 \cdot ETOT$$

The distribution of this ξ variable is shown in Fig. 9 for protons and for pions/muons. The subsample of pions/muons with $R^2 > 225$ mm^2 (that is dominated by muons) is also shown.

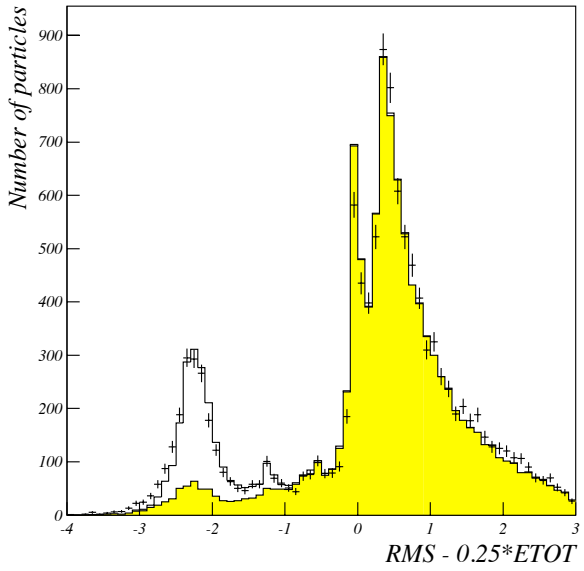

Figure 9: Distribution of the discriminating variable ξ for protons (yellow/shaded histogram), pions/muons (crosses), and for pions/muons with $R^2 > 225$ mm^2 (open histogram).

Fig. 9 suggests that

- the cut $\xi < -1.0$ will efficiently select muons;
- there is a background from sail-through hadrons, i.e., of hadrons that do not interact inelastically and look like muons.

Since protons are identified by the beam instrumentation, the background of sail-through protons can be measured directly. However, what is needed is the sail-through probability of pions which is different from the one of protons and cannot be measured with the beam instrumentation.

When starting from the well-determined sail-through probability of protons, only the ratio of the pion and proton sail-through probabilities is needed, so advantage is taken of the error cancellation in the ratio.

Moreover, all complications from detailed Monte Carlo simulations of proton and pion showers are avoided by asking for the ratio of probabilities that protons and pions do not interact inelastically and therefore look muon-like.

In order to end up near $\xi = -2.5$, protons and pions are not to interact in about 80 cm of iron[3]. With the interaction lengths of protons and pions of 18 cm and 21 cm, respectively, the non-interaction probabilities are 0.011 for protons, and 0.022 for pions. In other words, the sail-throuph appearance of pions is twice the sail-through appearance of protons.

The pion fraction is therefore determined by the number of events with $\xi < -1.0$ for pion/muon beam particles, minus the sail-through background of pions which is twice the observed number of protons with $\xi < -1.0$.

There is one more correction to apply to get the fraction of muons at the target which is needed for the cross-section normalization: the number of pion decays into muons between the target and the beam-muon identifier must be subtracted. The calculation of this background is straightforward.

7 Muon fraction in T9 pion beams

The fraction of muons must be measured within the same acceptance cut in the impact radius at the target that is used to produce the physics results. Throughout this memo, we use the cut

$$R < 12 \text{ mm} .$$

With the procedure outlined above, we obtain the fraction of muons to the sum of pions and muons listed in Table 2, for the beam momenta used in HARP data taking.

Table 2: Our ('HARP–CDP's) fractions of muons to the sum of pions and muons; for comparison, also the ones from 'official' HARP are shown.

Beam momentum [GeV/c]	HARP–CDP	'Official' HARP
± 3.0	$(4.1 \pm 0.4)\%$	$(4.2 \pm 0.5)\%$
± 5.0	$(5.1 \pm 0.4)\%$	$(5.2 \pm 0.6)\%$
± 8.0	$(1.9 \pm 0.5)\%$	$(4.1 \pm 0.8)\%$
$+8.9$	$(1.7 \pm 0.5)\%$	$(2.02 \pm 1.0)\%$
± 12	$(0.6 \pm 0.6)\%$	$(2.82 \pm 1.0)\%$
$+12.9$		$(2.52 \pm 1.0)\%$
± 15	$(0.0 \pm 0.5)\%$	

'Official' HARP's analysis method rests on Monte Carlo simulation of hadronic showers in a way that is not in line with established experimental knowledge. Since the absorption length of pions is larger by $\sim 15\%$ than the absorption length of protons, it cannot be correct that

[3]The overall length of 115 cm of the beam-muon identifier is not the relevant depth of iron; when the hadron interacts shortly before exiting from the beam-muon identifier, it may for a short distance produce three charged particles and still end up in the 'muon peak' of the ξ variable.

'...the punch-through contributions for pions and protons...were found to be similar within 20%'.

References

[1] A. Kayis-Topaksu and J. Panman, Determination of the muon contamination in the T9 beam, HARP memo 06-004 (2006)